Archives of Hydro-Engineering and Environmental Mechanics 71 (2024), pp. 123–134, doi: 10.2478/heem-2024-0008

sciendo

Archives of Hydro-Engineering and Environmental Mechanics

Published since 1954

ISSN 1231–3726

Three-dimensional Analysis of a Tunnel Excavation in a Jointed Rock Mass

Lesław Zabuski

Institute of Hydro-Engineering, Polish Academy of Sciences, Kościerska 7, 80-328 Gdańsk, Poland; e-mail: lechu@ibwpan.gda.pl

(Received 12 November 2024; revised 27 December 2024)

Abstract. A tunnel at a shallow depth, lying between several and 55 meters, was excavated in a jointed rock mass. Models of the rock mass and tunnel were elaborated basing on the data from an object in Carpathian flysch (Poland). The tunnel behaviour was analysed by using FLAC3D program and Coulomb-Mohr criterion and ubiquitous model of the rock mass with 10 combinations of the joint systems orientation (with respect to the tunnel axis). The tunnel shape is horse-shoe and its height equals 4.5 m. In each tunnel cross-section, 16 rock bolts and 20 cm shotcrete layer (with the strength increasing with time) were mounted. In cases of unfavourable orientation of joint system and unstable conditions, rock bolting of the tunnel heading face was installed and modelled. The numerical analysis was carried out for each excavation step, equal to 1.5 m. The entire deformation process and stress redistribution were registered starting with the cross-section in originally intact rock mass (i.e. before the tunnel heading face reached it), to the section located far from the face, in already supported and stabilized tunnel. The results obtained show the effect of discontinuities orientation on the stress distribution and displacement magnitude. The first signs of tunnel approaching heading face appear in a cross-section situated in a distance of 7 to 9 m from it. The processes of stress and displacement redistribution are long-range and occur in a distance of many meters from the already excavated tunnel face. The important result of the analysis was the determination of the ground response curves representing decompression and support loading as a function of the excavation advance. These results allow for better design of a proper support system of the tunnel.

Key words: Carpathian flysch, tunnel, 3D numerical calculations, displacement, stress distribution

1. Introduction

Tunnel excavation causes deformations of a rock mass and stress redistribution in three-dimensions. Reduction of the problem to two dimensions (2D), i.e. to the plane state, as is usually done (e.g. Brown et al 1983, Vlachopoulos and Diederichs 2014, Oke et al 2018, Karakus 2007, Kabwe et al 2020, Li et al 2020, Wang et al 2012, Mohammad Reza Zareifard 2021, Zamora Hernandez et al 2019, Kyung-Ho et al 2008) significantly simplifies the designing of a tunnel. However, such an approach does not enable taking into account some processes, as e.g. a favourable supporting effect of the tunnel heading face or intact rock mass decompression in the space ahead of this face (Zamora Hernandez et al 2019, Wang et al 2012). The latter phenomenon causes reduction of the pressure acting on the tunnel support, and in consequence, it allows for the reduction of its dimensions (Karakus and Fowell 2003). However, this is not considered in 2D solutions, or is estimated only approximately (Vlachopoulos and Diederichs 2014). Another problem concerns increasing pressure acting on the support in the cross-sections of the tunnel, located at a long distance from the heading face.

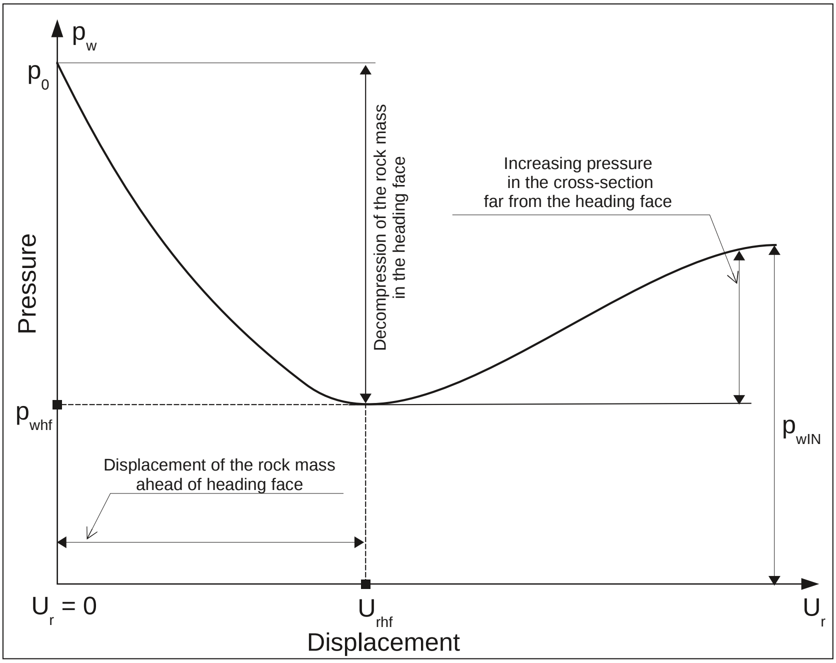

Fig. 1. Idealized ground response curve (GRC) during the tunnel excavation

The schematic ground response curve (GRC) shown in Figure 1 illustrates the problem presented above. Pressure p_o denotes hydrostatic pressure on the tunnel level. The pressure changes, i.e. decreases when the tunnel lies near the considered cross-section and the pressure encumbers the support in the heading face equals only p_{whf}, i.e. it is much lower than the initial one. Thanks to this phenomenon, the dimensions of the tunnel support can be more economically designed (Brown et al 1983, Oke et al 2018). The pressure increases again when the excavation works are continued, as the static loading begins to play some role, so that finally the support is loaded by the pressure p_{wIN}. Some authors considered the part of displacement U_{rhf}, e.g. Egger (1981) analyzed different rock mass conditions and excavation techniques, and recognized that U_{rhf} changes between 5% and 70–80% of the final convergence (for time $t = \infty$) depending mainly on the quality of the rock mass.

The above explanations can lead to the conclusion that the satisfactory, quantitative description of these processes is only possible if the results from a 3D analysis are available and taken into account.

The author analysed the behaviour of a tunnel under construction (Zabuski 2006). He elaborated the models of the rock mass and tunnel on the base of data coming from the object that was constructed in the Carpathian flysch in the south of Poland (Thiel 1989, Malata 2008, Książkiewicz 1977, Zabuski 2002). The rock mass is composed of weak and soft clay shale layers and relatively hard sandstones (Malata 2008, Zabuski 2002). The depth of the tunnel ranges between 5 and 55 m and numerical simulation of the tunnel be-haviour was done for a depth of the tunnel bottom level equal to 35 m. The calculations were carried out using the FLAC3D program (Itasca 1998). The numerical simulation was performed based partially on the numerical procedure described in the program manual. However, numerous substantial modifications were introduced in the original model.

2. Modelling of the Rock Mass and the Support of Tunnel

The model is fixed in the vertical X-Z planes in the Y direction, and in the planes Y-Z in the X, and in the X-Y plane (base) in the Z directions (Fig. 2).

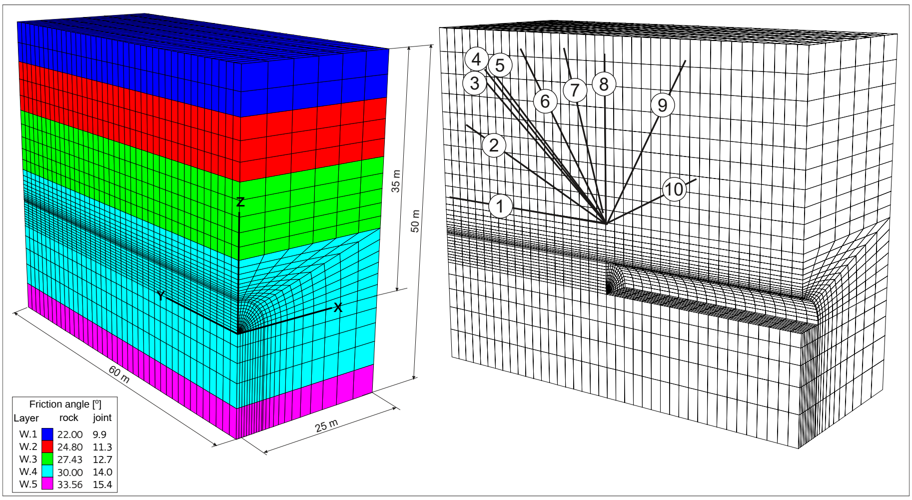

Fig. 2. Model of the tunnel; (a) geometry of the model; (b) orientation of joint sets in ubiquitous model: 1 – 0°/0°, 2 – 180°/30°, 3 – 180°/45°, 4 – 180°/47°, 5 – 180°/48°, 6 – 180°/60°, 7 – 180°/75° A, B, 8 – 0°/90°, 9 – 0°/60°, 10 – 0°/30°

Rock mass is modelled as an elastic-ideally plastic or ubiquitous body, obeying the Coulomb-Mohr failure criterion and a non-associated flow rule. Ten orientations of joint sets are considered in the ubiquitous model (Hu et al 2022, Li et al 2020). The intact rock is isotropic; the anisotropy results from the presence of the preferred direction of failure along the joints – so called "tectogenetic" anisotropy (Zabuski 2002). The rock mass is divided into 5 layers (Fig. 2a). Cohesion and tension strengths are equal to zero in all cases, whereas the friction angle in both rock and joints changes, increasing with depth as the quality (strength) of the medium increases (see Fig. 2a).

The tunnel support consists of a shotcrete layer and rockbolts which are uniformly distributed around the tunnel perimeter in its cross-section, and their spacing along the tunnel axis equals 1.5 m. The parameters of rockbolts are as follows:
Steel bolt: length L_k = 3.0 m; diameter d = 22 mm; borehole diameter D = 38 mm; steel elasticity modulus E_{st} = 21 GPa; steel unit weight γ_{st} = 78 kN/m^3; maximum tension force P_r = 118 kN.
Contact steel-cement-rock: joint cohesion = 55 kN (joint cohesion means cohesion along unit length of the borehole); shear stiffness = 10 GN/m/m (shear stiffness is the force, producing unit shear displacement along the unit length of the contact).

Characteristics of the shotcrete layer are as follows: thickness d_{bn} = 20 cm; unit weight γ_{bn} = 25 kN/m^3, elasticity modulus E_{bn} = 15 GPa; Poisson's coefficient ν_{bn} = 0.2.

The "slices" of the material 1.5 m thick were excavated and removed step by step during the simulation. The support was installed immediately after the excavation of each slice and the calculations were continued, until an equilibrium state was reached.

In cases of joint orientations 180°/48°, 180°/60° and 180°/75°A, B, when the joints inclination was greater than 47°, the heading face collapsed. It was thus necessary to install the bolting in the space of the tunnel face. The dimensions and bolts parameters were the same as above described. Their number increased with the increasing inclination of joints (Fig. 3).

3. Presentation and Analysis of the Simulation Results

Special attention is paid to three groups of 3D results, which cannot be accurately taken into account in a 2D analysis, namely:
- displacements in the direction of the longitudinal axis (Y) of the tunnel;
- stresses in the neighborhood of the heading face;
- ground response curves (Brown et al 1983) and support loading curves.

3.1. Displacements

Figure 4 presents the calculated displacement vectors and the fields of the horizontal displacement in the Y direction for selected orientations of joint sets in the vicinity of the tunnel heading face. Relatively high uplift of the tunnel bottom occurs where the joints are directed towards the rock mass (see Fig. 4). The greatest displacement occur

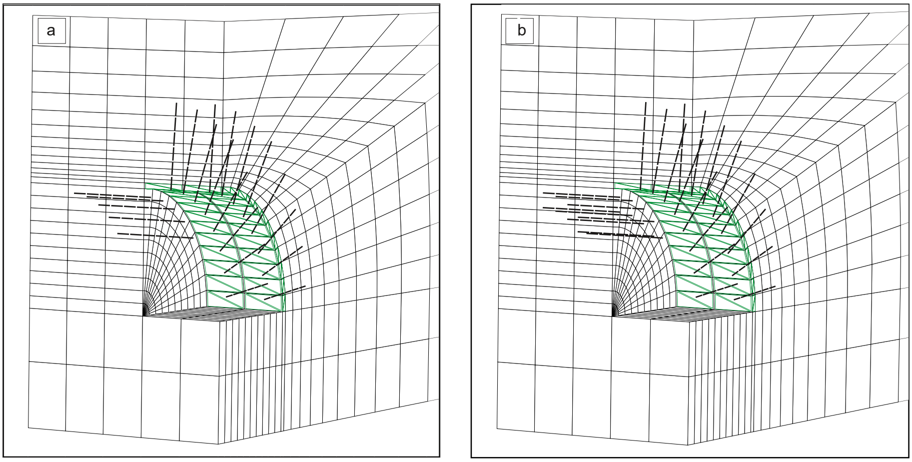

Fig. 3. Bolting of the tunnel heading face; (a) joint orientation 180°/48°: 5 bolts, (b) joint orientation 180°/60° and 180°/75°A: 9 bolts (in case 180°/75°B: 11 bolts)

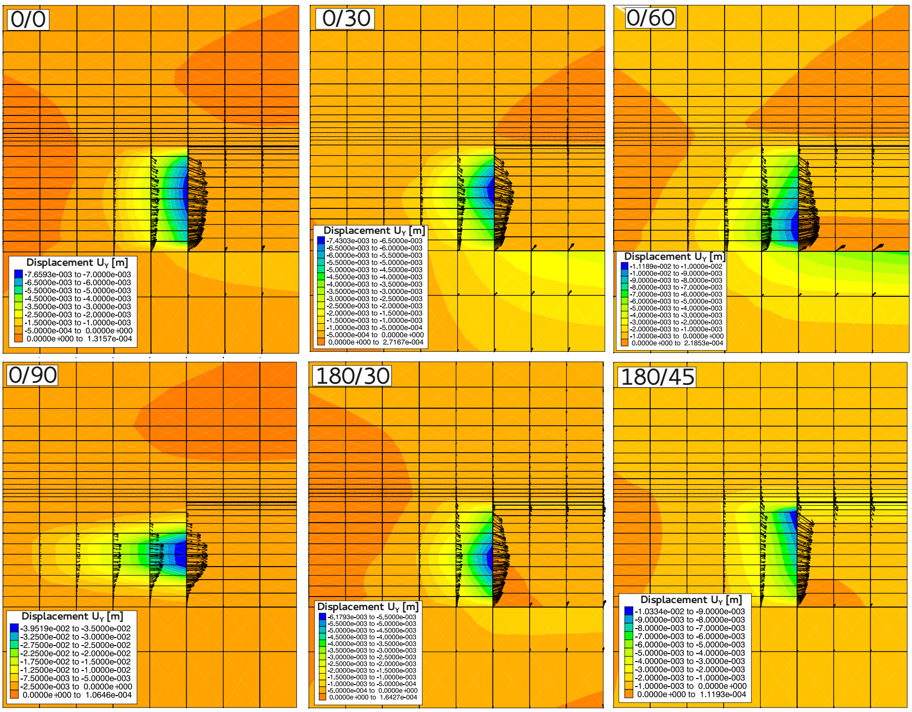

Fig. 4. Field of horizontal displacement U_Y and displacement vectors (cases without bolting of heading face)

in the case of perpendicular joints. In this case the rock mass begins to deform in the direction of the tunnel as early as about 6–7 m from the heading face and maximum displacement in central part of the face is almost four or more times greater than in other cases. It is also worth mentioning that vertical displacement in this case is very small.

It can be seen that the steeper the dip angle of joints the greater U_Y displacement of the heading face. The position of the maximum displacement vector depends on the joint orientation as well. In the majority of the presented cases it is located in the central part of the face, except for two cases in which the joints are inclined relatively steeply. It is also worth mentioning that the vectors in both the roof and bottom are directed outwards of the face.

As was mentioned in a former chapter, collapse of the heading face was observed when the joints were directed towards the tunnel space and their dip angle was greater than 47°. Stabilization was reached in such cases thanks to the installation of rockbolts (see Fig. 3). Four cases are shown in Figure 5. The maximum displacement vector is located between the central and upper part of the face. Bottom displacement is almost negligible and roof displacement vectors are directed outwards of the heading face. The difference of the dis-placement magnitude between the cases 180/75A and 180/75B is noteworthy. They differ in the number of the rockbolts – there are 9 bolts in case A and 11 in B. Despite this small difference, displacement in the latter case is noticeably smaller than in the first one (Fig. 6a); this shows the high efficiency of face bolting. Not only the number but also the position of the bolts is important and influences their efficiency. In Figure 6b forces in rock-bolts supporting the heading face are shown. Some bolts are compressed and this is at variance with the assumption that the bolt is tensioned. In fact, they should be repositioned and placed in the lower portion of the face. This example shows the efficiency of a 3D analysis and its potential in some situations.

3.2. Stresses

The stress distribution in both the vicinity of the heading face and far from it is noticea-bly different from that determined in a 2D analysis. The stress components change be-tween the cross-section in the rock mass ahead of the heading face (NAT) and the cross-section in the excavated tunnel, located far from the face (INF).

Table 1 illustrates the changes in the stress components at three stages (NAT, HF, INF) of the excavation. The stress redistribution between these stages is similar in all cases and some differences have a minor significance. Component σ_x in cases of steeply inclined joints decreases almost twofold between NAT and HF and increases approximately two-fold between HF and INF independently of the joint orientation. It is almost equal to the magnitude in a natural state of stress. Component σ_z significantly decreases from NAT to INF whereas component σ_y decreases from NAT to HF and then increases between HF and INF.

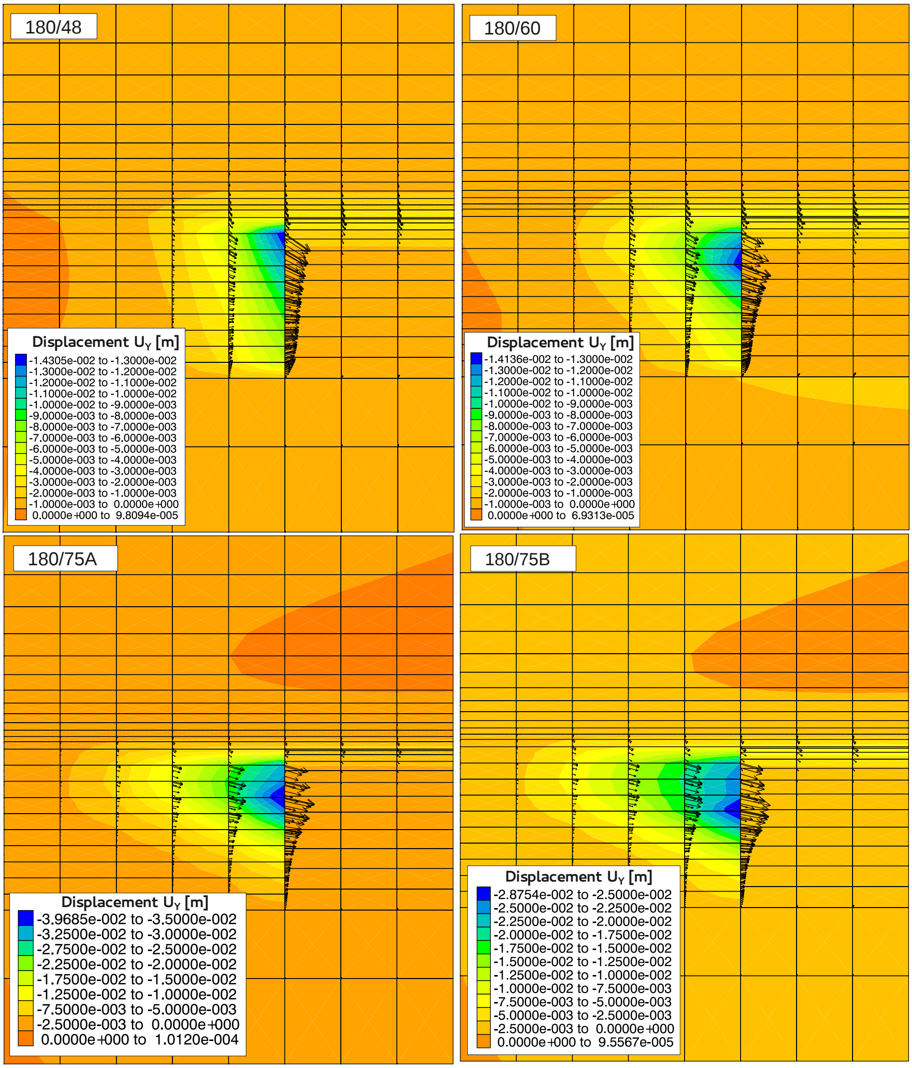

Fig. 5. Field of horizontal displacement U_Y and displacement vectors (cases with bolting of heading face)

The stress distribution in the support element located in the roof zone is shown in Figure 7. As can be seen, the smallest values develop in the rock mass near the heading face and then all the three components increase.

The components σ_x and σ_z are almost constant in the cross-sections lying far from the face (HF), whereas σ_y constantly rises. The deviatoric $(\sigma_x - \sigma_z)$ stress is the largest in each cross-section along the considered length of the tunnel. It means that failure in the roof is possible first of all in the X-Z plane, i.e. in the plane of the cross-section which is perpendicular to the longitudinal axis of the tunnel.

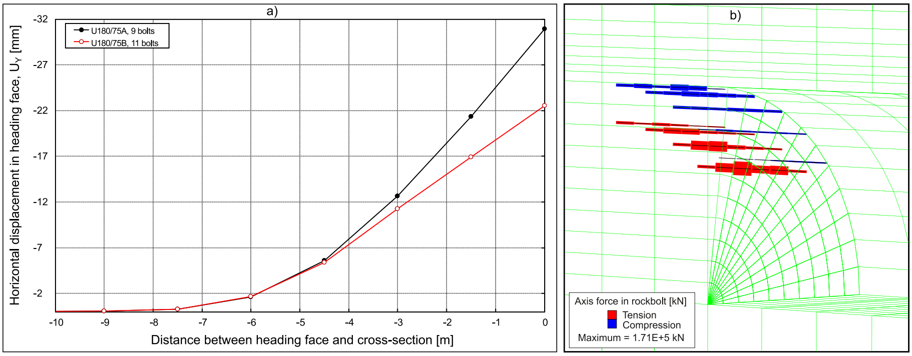

Fig. 6. Influence of rockbolts supporting tunnel heading face; (a) U_Y in rock mass ahead of heading face; (b) distribution of axial forces in rockbolts (180/75A)

Table 1. Stress components in the roof zone above the contact between rock mass and support

Model	Stage (position of the cross-section)	Stress					
		σ_x [kPa]	σ_y [kPa]	σ_z [kPa]	σ_x/σ_y	σ_y/σ_z	σ_x/σ_z
	Natural; NAT	−431	−389	−748	1.11	0.52	0.58
0°/0°	Heading face; HF	−339	-206	−111	1.65	1.86	3.05
	Far from HF; INF*	−515	−287	−226	1.79	1.27	2.28
	Natural; NAT	−410	−521	−718	0.79	0.73	0.57
180°/45°	Heading face; HF	−185	−171	−91	1.08	1.88	2.04
	Far from HF; INF	−392	−99	−181	3.97	0.55	2.17
	Natural; NAT	−410	−527	−713	0.78	0.74	0.58
180°/47°	Heading face; HF	−194	−101	−91	1.92	1.11	2.14
	Far from HF; INF	−399	−213	−180	1.87	1.18	2.22
	Natural; NAT	−394	−382	−696	1.03	0.55	0.57
180°/75°B	Heading face; HF	−195	−125	−64	1.56	1.97	3.07
	Far from HF; INF	−360	−240	−154	1.50	1.56	2.34
	Natural; NAT	−390	−359	−686	1.09	0.52	0.57
0°/90°	Heading face; HF	−183	−141	−58	1.30	2.44	3.17
	Far from HF; INF	−348	−275	−144	1.27	1.91	2.42
	Natural; NAT	−403	−490	−694	0.82	0.71	0.58
0°/60°	Heading face; HF	−230	−114	−70	2.02	1.63	3.29
	Far from HF; INF	−3.71	−153	−157	2.42	0.97	2.36

* HF – heading face, INF – "infinity"

3.3. Decompression of the Rock Mass and Loading of the Support

The rock mass decompression of can be expressed by GRC (see Fig. 1). As it was explained earlier GRC represents the relationship between the pressure exerted on the support by the rock mass and its radial displacement, i.e. convergence. The authors who first proposed this approach were Fenner and Pacher (in Müller 1978). Next, numerous authors presented different approaches enabling GRC determination

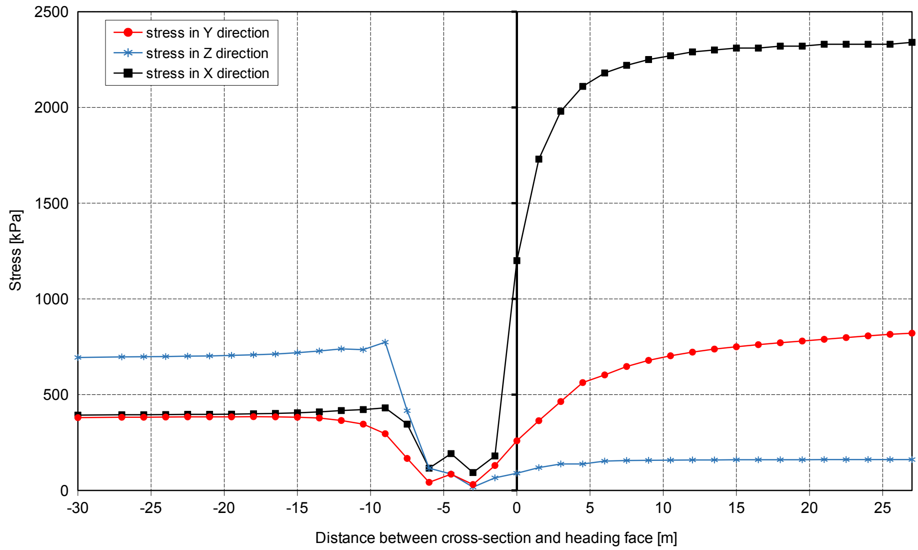

Fig. 7. Changes of the stress components in the tunnel support – roof zone

in plane strain condi-tions (e.g. Brown et al 1983, Sulem et al 1987, Labiouse 1996, Kyung-Ho et al 2008). Decompression of the rock mass is accompanied by its loosening. the rock mass is self-supporting ahead of the heading face and temporarily in inside the rock mass. However, in the cross-sections located at some distance from the face, tunnel support is necessary, especially in cases of weak rock mass where plastic deformations appear. The support acts against the decompressed mass and deforms accordingly. Thus, the curve shown in Figure 1 should be supplemented by the curve of support loading. Yet, it is impossible to find the point of the support installation on the abscissa (displacement) axis in 2D analysis, although some authors tried to find a solution (Reed 1988, Egger 1981, Yamamoto et al 1991). 3D analysis makes possible the determination of this point and the drawing of en-tire curves of the joint support-rock mass displacement-pressure relationship.

Four examples of GRC and support loading curves are shown (Figs. 8 and 9). Figure 8 presents the curves for cases of steeply inclined joints with heading face bolting. As can be seen, thanks to decompression, vertical pressure acting on the support decreases more than seven-fold in the vicinity of the wall face and more than fourfold in the cross-section far from it, as compared with the pressure in the natural conditions. The face bolting has no influence on the pressure, but the displacement in case 75A (9 bolts) is somewhat greater than in 75B (11 bolts).

The relation of the curves in Figure 9 looks different. The displacement is almost identical, whereas the pressures differ by more than 20%. Here the joints dip almost identically, yet the heading face in the case 180°/48° is bolted. The pressure reduction in the support (as compared with the natural state) is similar to the case described above.

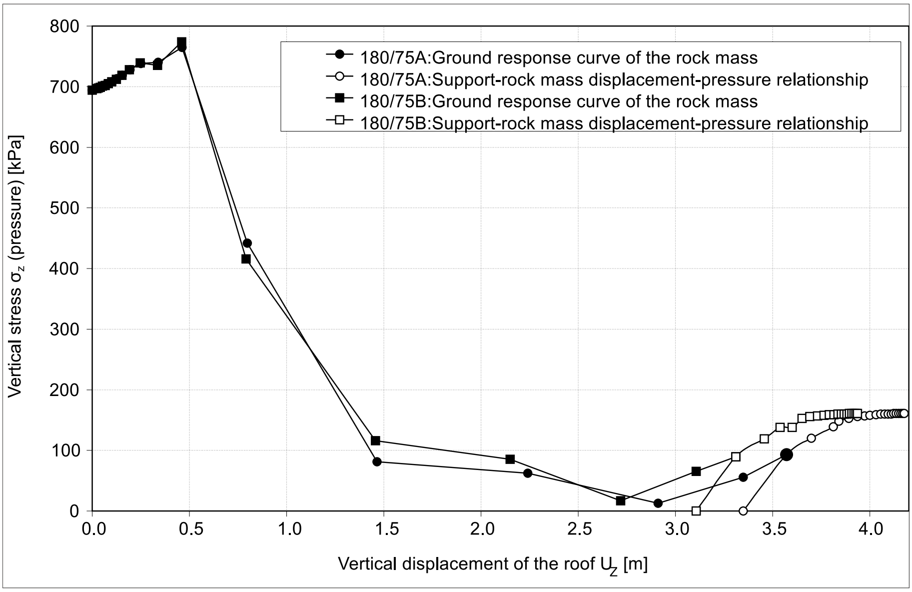

Fig. 8. Models 180°/75°A, B. Ground response and support loading curves

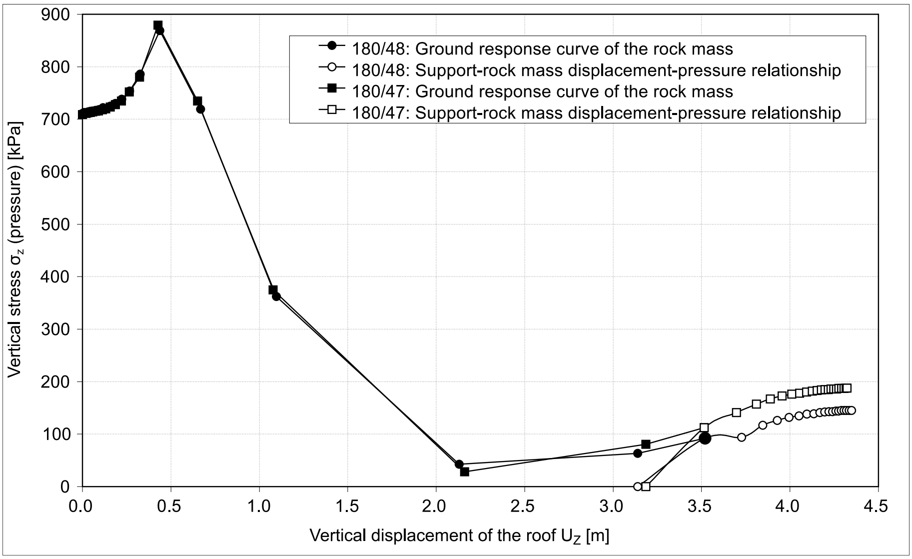

Fig. 9. Models 180°/47°, 180°/48°. Ground response and support loading curves

4. Summary and Conclusions

The paper has a partially "methodological" character. Based on the results of a 3D analysis, the tunnel behaviour being under construction was described. It should be pointed out that only general data from a real tunnel excavated in the Carpathian flysch was taken into account in the analysis. There are numerous phenomena developing during the tunnel excavation stage, and the behaviour in the direction of the tunnel longitudinal axis (i.e. Y) was specially emphasized.

The analysis of the effect of the joint sets orientation on the stress distribution and displacement fields show that the most unfavourable joints arrangement is that when the joints are steeply inclined and dip inside the tunnel space. In some cases, in which the joints are inclined at an angle greater than 47° to the horizontal direction, the installation of the heading face bolting is necessary. It is also shown that the stress component in the Y direction is relatively high, but the greatest deviatoric stress develops in the X-Z plane, which is the plane of the potential failure.

An important part of this paper was devoted to the determination of the ground response curves and support loading curves. It was shown that a 3D approach enables the determination of these curves without additional doubtful assumptions, while taking into account the effect of the rock mass decompression occurring prior to the installation of the support.

References

Brown E.T., Bray J.W., Ladanyi B., Hoek E. (1983) Ground response curves for rock tunnels, *Journal Geotechn. Eng. ASCE*, **109**(1), 15–39 (doi: 10.1061/(ASCE)0733-9410(1984)110:1(140)).

Egger P. (1981) Deformations au front de taille. Determination de la cohesion du massif rocheux, *Revue Francaise Geotechnique*, **4**.

Hu Z., Wu B., Xu N., Wang K. (2022) Effect of discontinuities on the stress redistribution and rock failure: A case of underground caverns, *Tunnelling and Underground Space Technology*, **127**, 104583 (doi: 10.1016/j.tust.2022.104583).

Itasca C.G. (2000) *Flac 3D Manual*, Minneapolis.

Kabwe E., Karakus M., Chanda E.K. (2020) Proposed solution for the ground reaction of non-circular tunnels in an elastic-perfectly plastic rock mass, *Computers and Geotechnics*, **119**, 103354 (doi.org/10.1016/j.compgeo.2019.103354).

Karakus M. (2007) Appraising the method accounting for 3D tunnelling effect in 2D plane strain FE analysis, *Tunnelling and Underground Space Technology*, **22** (1), 47–56 (doi.org/‘10.1016/j.tust.2006.01.004).

Karakus M., Fowell R.J. (2003) Effect of different tunel face advance excavation on the settlement by FEM, *Tunnelling and Underground Space Technology*, **18** (5), 513–523 (doi.org/10.1016/S0886-7798(03)00068-3).

Książkiewicz M. (1977) Tectonics of the Carpathians, [in:] Pożaryski W. eds. Vol. IV *Tectonics*, Wydawnictwo Geologiczne, Warszawa, 476–609.

Kyung-Ho P., Bituporn Tontavanich, Joo-Gong Lee (2008) A simple procedurę for ground response curve of circular tunel in elastic-strain softening rock mass, *Tunneling and Undergound Space Technology*, **22** (2), 151–159 (https://doi.org/10.1016/j.tust.2007.03.002).

Labiouse V. (1996) Ground response curves for rock excavations supported by ungrout-ed tensioned rockbolts, *Rock Mechanics and Rock Engineering*, **29** (1), 19–38.

Li A., Liu Y., Dai F., Liu K., Wei M. (2020) Continuum analysis of the structurally controlled displacements for large-scale undergound caverns in bedded rock masses, *Tunnelling and Underground Space Technology*, **97**, 103288 (doi: 10.1016/j.tust.2022. 103288).

Malata T. (2008) Development of Polish Flysch Carpathians revealed in outcrops and landslide, *Przegląd Geologiczny*, **56** (8/1), 688–691.

Mohammad Reza Zareifard (2021) Ground response curve of deep circular tunel in rock mass exhibiting Hoek-Brown strain-softening behaviour considering the dead weight loading, *European Journal of Environmental and Civil Engineering*, **25** (14).

Müller L. (1978) *Der Felsbau*, 3-er Band: *Tunnelbau*, Stuttgart: Enke-Verlag.

Oke J., Vlachopoulos N., Diederichs M. (2018) Improvement to the Convergence-Confinement Method: Inclusion of Support Installation Proximity and Stiffness, *Rock Mechanics and Rock Engineering*, **51**, 1495–1519.

Reed M.B. (1988) The influence of out-of-plane stress on plane problem in rock mechanics, *Int. Journal Num. & Anal. Meth. in Geomechanics*, **12** (2), 173–181.

Sulem J., Panet M., Guenot A. (1987) Closure analysis in Deep Tunnels, *Int. Journal Rock Mech. Min. Sci. Abstr.*, **24** (3), 337–345.

Thiel K. (1989) *Rock Mechanics in Hydroengineering*, PWN Warszawa, Ensevier Amsterdam-Oxford-New York-Tokyo.

Vlachopoulos N., Diederichs M. (2014) Appropriate uses and practical limitations of 2D numerical analysis of tunnels and tunnel support response, *Geotechnical and Geological Engineeing*, **32** (2), 469–488.

Wang X., Kulatilake P., Song W. (2012) Stability investigations around a mine tunnel through three-dimensional discontinuum and continuum stress analysis, *Tunnelling and Underground Space Technology*, **32**, 98–112.

Yamamoto J., Mogi G., Yamaguchi U. (1991) Three-dimensional supporting effect of tunnel face, [in:] Beer, Booker Carter (eds.), *Computer Methods and Advances in Geomechanics*, 1527–1532, Rotterdam-Boston: Balkema.

Zabuski L. (2006) *Trójwymiarowa analiza zachowania się tunelu w masywie skalnym w trakcie drążenia tunelu* (in Polish), Polish Academy of Sciences, Institute of Hydro-Engineering, Int, report.

Zabuski L. (2002) *Zachowanie się fliszowego ośrodka skalnego w otoczeniu konstrukcji podziemnej (na przykładzie tunelu na niedużej głębokości)* (in Polish), Institute of Hydro-Engineering, Gdańsk, 262 p.

Zamora Hernandez Y., Durand Farfan A., Pacheco de Assis A. (2019) Three-dimensional analysis of excavation face stability of shallow tunnels, *Tunnelling and Underground Space Technology*, **92**, 103062 (doi.org/10.1016/j.tust.2019. 103062).